Numerical modeling of molecular diffusion and convection effects during gas injection into naturally fractured oil reservoirs

Hossein Gholamian, Mohammad Reza Ehsani, Mohammad Nikookar, Amir H. Mohammadi

Oil & Gas Science and Technology – Rev. IFP Energies nouvelles **76**, 81 (2021)

https://doi.org/10.2516/ogst/2021065

Available online at:
ogst.ifpenergiesnouvelles.fr

REGULAR ARTICLE

OPEN ACCESS

Numerical modeling of molecular diffusion and convection effects during gas injection into naturally fractured oil reservoirs

Hossein Gholamian[1], Mohammad Reza Ehsani[1], Mohammad Nikookar[2], and Amir H. Mohammadi[3,*]

[1] Department of Chemical Engineering, Isfahan University of Technology, 8415683111 Isfahan, Iran
[2] Improved Oil Recovery (IOR) Research Institute, National Iranian Oil Company (NIOC), Vanak Square, Tehran, Iran
[3] Discipline of Chemical Engineering, School of Engineering, University of KwaZulu-Natal, Howard College Campus, King George V Avenue, Durban 4041, South Africa

Received: 12 July 2021 / Accepted: 15 November 2021

Abstract. Gas injection into a naturally fractured oil reservoir keeps the reservoir pressure and increments the initial recovery from the reservoir. The main aim of this work was to develop a numerical model to calculate the mass transfer (molecular diffusion and convection) between a gas injected in the fracture and residual fluid (gas and oil) in a matrix block. The dual continuum model is applied to describe flow behaviour and fluid recovery in porous media. Finally, the model is validated by comparing the outcomes with the results of two experimental works available in the literature. The mathematical model results are in agreement with the laboratory data including recovery of each component, saturation profile, and the pressure gradient between matrix and fracture. Modeling results show that after 25 days of N_2 injection, the lighter and heavier components (C1 and C5) are recovered about 51% and 39%, respectively. These amounts for CO_2 injection are 49% and 27%. It is found that the convection mechanism has a great effect on preventing the pressure drop of the reservoir during injection operations. In the nitrogen injection, without considering the convection, after 30 days, the matrix pressure reaches 1320 Psi from 1479 Psi but after 30 days, considering the convection, the pressure reaches 1473 Psi from 1479 Psi.

Nomenclature

A	Area, m^2
C	Concentration, mol/m^3
c	Component
D	Depth, m
$D_{c,o}$, $D_{c,g}$	Diffusion coefficient of component c in oil and gas, cm^2/s
D_g	Diffusion coefficient of gas, cm^2/s
$f_{o,c}$, $f_{g,c}$	Fugacity of component c in oil and gas, Psi
H	Thickness of fracture in z-direction, m
k	Permeability, md
k_c	Diffusion mass transfer coefficient of component c at matrix-fracture boundary, $mole/(m^2\ s)$
k_{ro}, k_{rg}, k_{rw}	Relative permeability of oil, gas, and water
l	Length of fracture, m
MW_i	Molecular weight of component I, g/gmol
n_c	Components Number
$Nc,\ p$	Molar flux of diffusion for component c at phase p, $mole/(m^2\ s)$
P_{cog}, P_{cow}	Capillary pressure (oil–gas and oil–water), Psi
p	Pressure, Psi
p_o, p_g, p_w	Pressure of oil, gas, and water, Psi
Δp	Gradient of Pressure, Psi/ft
$q_{D,fm,c}$	Diffusion mass transfer rate of component c at the matrix-fracture boundary, mole/s
$q_{C,fm,c}$	Convection mass transfer rate of component c at the matrix-fracture boundary, mole/s
q	Flow rate, ft^3/day
S_o, S_g, S_w	Saturation of oil, gas, and water
t	Time, day
T	Temperature, K
$\bar{v}$	Average velocity of gas stream in the fracture, m/s
v_o	Velocity of oil bulk, m/s
v_g	Velocity of gas bulk, m/s
v_x, v_y, v_z	Velocities of fluid bulk in x, y, and z directions, m/s

* Corresponding author: amir_h_mohammadi@yahoo.com

W	Width of fracture in y-direction, m
x, y, z	Cartesian coordinates
x_c	Mole fraction of component c in oil phase
$x_{i,m}$,$x_{j,m}$	Mole fraction of component i and j in phase m
y_c	Mole fraction of component c in gas phase
$y_{c,\,mf}$	Mole fraction of component c in the gas phase at matrix-fracture boundary
$y_{c,f}$	Mole fraction of component c at the entrance of the fracture
Z_c	Overall composition of c

Greek

Δx,Δy,Δz	Grid cells dimensions, m
$\gamma_o, \gamma_g, \gamma_w$	Specific gravity of oil, gas, and water, psi/ft
μ_o, μ_g, μ_w	Viscosity of oil, gas, and water, cp
ϕ	Porosity
ρ_o, ρ_g, ρ_w	Molar densities of oil, gas, and water, mole/cm^3

1 Introduction

The major parameter for production from heavy oil reservoirs is high oil viscosity [1–3]. Gas injection into a naturally fractured oil reservoir not only maintains the reservoir pressure but also increases the reservoir initial recovery [4–8]. When gas is injected into an unsaturated fractured reservoir, the gas enters both fracture and matrix media [9, 10]. It causes oil to swell and move from the matrix [11–15]. Furthermore, injected gas in the matrix causes some components of oil to evaporate and move to the gas phase. Therefore, oil is transported by both convection and diffusion mechanisms. Moreover, increasing the mobility of heavy oils by reducing their viscosity can be improved by injecting diluents such as gases. A lot of studies about injecting diluent gas have been carried out [11, 16–18]. The studies reveal that the diffusion of CO_2 into the core accounts oil to swell and subsequently reduce the viscosity which results in a higher gravity drainage rate [19, 20]. Also, dissolving gas in oil causes the oil to expand and reduce its density, and thereby the oil exits from the rock. Moreover, when liquid and gas phases are not in equilibrium, one or more components move from one phase to another one due to molecular diffusion [4, 11, 21–24]. The presence of dual porosity including porous media (low permeability/high porosity) and fracture networks (high permeability/low porosity) with different physical properties causes the structure of fractured reservoirs much more complex than conventional non-fractured reservoirs so that conventional methods which have been used for studying the performance of the reservoirs cannot present appropriate results to examine the behavior of reservoirs [10, 14, 25].

The molecular diffusion has been presented by Ertekin *et al.* [26]. Multiple mechanisms of fractured gas reservoirs have been considered by Ayala *et al.* [27], and they concluded that, unlike conventional reservoirs, molecular diffusion in fractured reservoirs has an important role in gas injection into oil reservoirs and gas production from gas condensate reservoirs. Moreover, secondary recovery and tertiary recovery have been studied by Karimaie [28]. According to the study, diffusion has a strong effect on secondary and tertiary oil recoveries. In addition, a compositional model has been presented by Kazemi and Jamialahmadi [29]. In their work, it has been concluded that at an early stage, swelling of oil has occurred, and gravity drainage has been followed by a slow extraction mechanism that can recover the heavy and intermediate components. Diffusion coefficients of gas and oil are very important for any field simulation of a fractured reservoir. Moreover, CO_2 injection tests in systems of matrix/fracture by using a finely-gridded compositional simulator have been studied by Alavian [30], and a single matrix block has been represented to understand the impact of molecular diffusion on oil recovery by CO_2 injection in a fracture-matrix system. The outcome of his work shows that diffusion would have a crucial role in oil recovery, except at very low CO_2 injection rates. Hoteit [31] demonstrated analytically and numerically that classical Fick's law does not consider the total flux balance and is unable to take the correct direction of the diffusion flux in some situations. Moreover, a numerical model based on Fick's law has been suggested by him to predict the gas–oil transfer mechanism. In the suggested model, the gradient of chemical potential is considered as the driving force. Also, the implementation of the simulations that consider diffusion using various solution methods has been examined by Mohebbinia and Wong [32]. Also, optimal performance is achieved by the partially implicit approach. The simulation outcomes have revealed that constant diffusion coefficients may not predict an acceptable result during gas flooding and oil recovery might be overestimated or underestimated. It has been observed by Darvish *et al.* [33] for a higher porosity case that, the viscosity reduces later and the effect of the molecular diffusion on oil recovery will increase if the porosity of the matrix is big. Jin *et al.* [34] examined the CO_2 EOR process in tight reservoirs and concluded that it is preferred to inject CO_2 into the fractures. When CO_2 dissolves in oil, oil viscosity reduces and oil drains into the fractures. Experimental and field studies have shown that CO_2 has an important role in displacing oil in porous media via interfacial tension change, viscosity reduction, and subsequent reaction of carbonic acid with minerals as well as oil swelling [35, 36]. For many conventional and unconventional reservoirs including heavy oil extraction in VAPEX (VAPour EXtraction) process [37, 38] or oil extraction by solution-gas-drive [39], diffusion is an important parameter [4, 17, 29, 40–46].

Diffusion could be an important recovery mechanism in naturally fractured reservoirs while there are very few attempts to model diffusion and convection between a flowing gas through the fracture and oil and gas in the matrix. The first objective of this work was to mathematically model mass transfer between a gas phase in the fracture and oil and gas phases in the matrix in a single porosity model. There are several commercial models for modeling

naturally fractured reservoirs. These models are classified as follows: Dual porosity model, dual porosity/dual permeability model, and dual continuum model.

The dual continuum model is the model used for gas injection into naturally fractured reservoirs in this paper. The dual continuum approach is either the single-block model or the single-porosity model. This model will be examined in the following and finally, the proposed model will be validated with experimental data available in the literature.

2 Dual continuum theory

This theory is applied to model fractured reservoirs by considering a porous media as a single matrix block with an adjacent fracture. The fracture is considered a boundary condition for the matrix. This model is a good expression of the natural fracture reservoir because it considers the fluid flow between the matrix block and the fracture. Figure 1 shows an overview of this model. In this model, the matrix is separated but the fracture is not separated because the fracture acts as a boundary condition for the matrix.

Compositional simulators were created to study the oil recovery of a reservoir during the injection of gas. In the compositional simulation, it is supposed that the hydrocarbon phase and water phase are insoluble. So, the mass conservation equations are applied separately for hydrocarbon and water compounds. For the multi-phase compositional flow, viscosity, gravity, and capillary forces must be calculated. Moreover, if gas is injected, a diffusion mechanism should be taken into account to determine the mass transfer between phases. The equations governing the multiphase flow are presented below. In principle, these equations use the continuum equations for each component C for a volume ($\Delta x\ \Delta y\ \Delta z$):

See the equation (1) bottom of the page

3 Mechanisms of mass transfer

Generally, there are three main mechanisms for the transfer of fluids in porous media: convection molecular diffusion, and mechanical dispersion. In this model, the mechanical dispersion is ignored. Thus, component C can cross the boundary by convection and diffusion mechanisms.

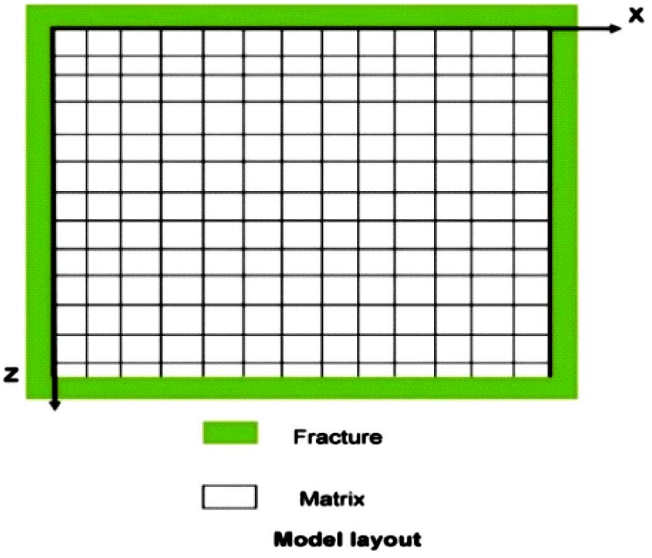

Fig. 1. Model view used in this work.

3.1 Convection mechanism

The mass transfer due to convection is a mechanism that components are displaced by the motion of the fluid mass. The potential gradient is the driving force for convection (bulk flow). Inlet molar rate (mole/time) minus the exit molar rate of component c in three directions by convection transfer in the gas and oil phase as below:

See the equation (2) bottom of the page

Using the mathematical form of Darcy's law:

$$\vec{v}_p = -\frac{kk_{rp}}{\mu_p}\left(\vec{\nabla} p_p - \gamma_p \overline{\nabla} D\right) \qquad p = \text{oil, gas.} \tag{3}$$

3.2 Molecular diffusion mechanism

Molecular diffusion is a mechanism that components are transferred by the random motion of molecules. Bird *et al.* [47] proved that for ideal or near ideal mixtures, gradients of concentration can be used instead of chemical potential gradients as the driving force. In this model, concentration gradient is considered as the driving force of molecular diffusion. If $N_{c,o}$ and $N_{c,g}$ (molar flux of

(Molar rate of component C accumulation) = (molar rate of component C input)– (molar rate of component C output)
+ (molar rate of component C injection)– (molar rate of component C production). (1)

$$\begin{aligned}&(\rho_0 x_c v_{o,x})|_x \Delta y\Delta z + (\rho_g y_c v_{g,x})\big|_x \Delta y\Delta z - (\rho_0 x_c v_{0,x})|_{x+\Delta x}\Delta y\Delta z - (\rho_g y_c v_{g,x})\big|_{x+\Delta x}\Delta y\Delta z+\\ &(\rho_0 x_c v_{0,y})_y \Delta x\Delta z + (\rho_g y_c y_{g,y})\big|_y \Delta x\Delta z - (\rho_0 x_c y_{o,y})\big|_{y+4y}\Delta x\Delta - (\rho_g y_c v_{g,y})_{y+4y}\Delta x\Delta z+\\ &(\rho_0 x_c v_{0,z})_z \Delta x\Delta y + (\rho_g y_c y_{g,z})\big|_z \Delta x\Delta y - (\rho_0 r_c v_{0,z})|_{z+\Delta z}\Delta x\Delta y - (\rho_g y_c y_{g,z})_{z+y_z}\Delta r\Delta y.\end{aligned} \tag{2}$$

component c) are expressed in mol/m^2 s (mol c/s per surface area) in oil and gas, these terms have mole units per surface area over time and indicate the amount of mass transfer by diffusion. Thus:

See the equation (4) bottom of the page

where

$$N_{c,o} = \phi S_o \rho_o (D_{c,0} \nabla x_c), \tag{5}$$

$$N_{c,g} = \phi S_g \rho_g (D_{c,g} \nabla y_c). \tag{6}$$

4 Flow equations

The flow equations could be acquired by substituting equations (2)–(6) in equation (1). Then, the obtained equations are divided by the volume of the element $\Delta x\ \Delta y\ \Delta z$ and applying limit, we will have:

$$-\left[\frac{\partial(\rho_o x_c v_{o,x} + \rho_g y v_{g,x})}{\partial x} + \frac{\partial(\rho_o x_c v_{0,y} + \rho_g y_c v_{g,y})}{\partial y} + \frac{\partial(\rho_o x_c v_{0,z} + \rho_g y_c v_{g,z})}{\partial z}\right]$$

$$-\left[\frac{\partial(N_{c,0,x} + N_{c,g,x})}{\partial x} + \frac{\partial(N_{c,0,y} + N_{c,g,y})}{\partial y} + \frac{\partial(N_{c,0,z} + N_{c,g,z})}{\partial z}\right]$$

$$+ q_{D,fm,c} + q_{c,fm,c} = \frac{\partial}{\partial t}\left[\phi(\rho_o S_0 x_c + \rho_g S_g y_c)\right]. \tag{7}$$

Or, in vector notation,

$$-\nabla \cdot (\rho_0 x_c v_0 + \rho_8 y_c v_g) - \nabla \cdot (N_{c,0} + N_{c,g}) + q_{D,ff,c} + q_{C,fm,c}$$

$$= \frac{\partial}{\partial t}\left[\phi(\rho_o S_0 x_c + \rho_g S_g y_c)\right], \tag{8}$$

where $q_{D,\ fm}$ and $q_{C,\ fm}$ are the diffusion and convection mass transfer between the matrix and the fracture at the fracture- matrix boundary based on mol/s, respectively. The sum of the fluid moles in the volume element at any time is: $\Delta x\ \Delta y\ \Delta z\ (\rho_o S_o + \rho_g S_g)\phi$.

And the mole of component c is equal to: $\phi(\rho_o S_o x_c + \rho_g S_g y_c)\ \Delta x\ \Delta y\ \Delta z$.

Therefore, the mole accumulation rate of component c is:

$$\frac{\partial}{\partial t}\left[\phi(\rho_o S_0 x_c + \rho_g S_g y_c)\right] \Delta x \Delta y \Delta z.$$

By substituting v_o and v_g from equation (3) and $N_{c,o}$ and $N_{c,g}$ from equations (5) and (6) into equation (8), it becomes:

$$\nabla \cdot \left(\rho_o x_c \frac{k k_{r0}}{\mu_o}\left(\vec{\nabla} p_o - \gamma_o \vec{\nabla} D\right) + \rho_g y_c \frac{k k_{rg}}{\mu_g}\left(\overline{\nabla}\, p_g - \gamma_g \overline{\nabla}\, D\right)\right)$$

$$+\nabla \cdot \left(\phi S_o \rho_o (D_{c.o} \nabla x_c) + \phi S_g \rho_g (D_{c,g} \nabla y_c)\right) + q_{D,fm,c} + q_{C,fm,c}$$

$$= \frac{\partial}{\partial t}\left[\phi(\rho_o S_0 x_c + \rho_g S_g y_c)\right] \qquad c = 1, 2, \ldots, n_c. \tag{9}$$

Equation (9) is the general state of the composite multiphase flow inside the porous medium for each component in the gas and oil phases in the porous medium. The first bracket shows the convection mechanism in the gas and oil phases. The mechanism of diffusion is shown in the second bracket. $q_{D,\ fm}$ and $q_{C,\ fm}$ are the mass transfer of diffusion and convection between the matrix and the fracture. A mass balance equation only expresses the movement of water by the convection mechanism because we assume that the hydrocarbon phase is insoluble in the water phase. Thus, for the water phase, we have:

$$\nabla \cdot \left(\rho_w \frac{k k_m}{\mu_w}\left(\overline{\nabla}\, p_w - \gamma_w \overline{\nabla}\, D\right)\right) = \frac{\partial}{\partial t}[\phi(\rho_w S_w)]. \tag{10}$$

The equations governing multi-phase compositional flow are derived from three sources:

1. The equilibrium equations of each component (Eq. (9)) and for water phase (Eq. (10)).
2. The phase equilibrium between the hydrocarbon phases is indicated as the below:

$$f_{o,c} = f_{g,c} \quad c = 1, 2, \ldots, n_c. \tag{11}$$

3. The auxiliary equations are the sum of the phase's saturation and the sum of the molar components in each phase is unity. Moreover, the oil, gas and water pressure should be related to the capillary pressure:

$$S_o + S_g + S_w = 1, \tag{12}$$

$$\sum_{c=1}^{nc} x_c = 1 \sum_{c=1}^{nc} y_c = 1, \tag{13}$$

$$P_{cog} = p_g - p_o,\ p_{cow} = p_o - p_w. \tag{14}$$

The equations that governing multiphase compositional flow in the porous media are expressed by equations (9)–(14). This system of equations contains a set of $(2n_c + 6)$ equations with the same number of unknowns as the below:

$$(p_o, p_g, p_w, S_o, S_g, S_w, x_1, x_2, \ldots, x_{nc}, y_1, y_2, \ldots, y_{nc}).$$

$$\begin{aligned}
&(N_{c,,x})|_x \Delta y \Delta z + (N_{c,g,x})|_x \Delta y \Delta z - (N_{c,,x})|_{x+\Delta x} \Delta y \Delta z - (N_{c,g,x})|_{x+\Delta x} \Delta y \Delta z \\
&+(N_{c,0,y})|_y \Delta x \Delta z + (N_{c,g,y})|_y \Delta x \Delta z - (N_{c,0,y})|_{y+\Delta y} \Delta x \Delta z - (N_{c,g,y})|_{y+\Delta y} \Delta x \Delta z \\
&+(N_{c,0,z})|_z \Delta x \Delta y + (N_{c,g,2})_z \Delta x \Delta y - (N_{c,0,2})|_{z+\Delta z} \Delta x \Delta y - (N_{c,g,z})|_{z+\Delta z} \Delta \Delta y,
\end{aligned} \tag{4}$$

5 Initial and boundary conditions

The initial and boundary conditions are presented next.

5.1 Initial conditions

It is supposed that there is gravity equilibrium in the model at time equal to zero. Also, pressure and composition at a reference are known. Since there is gravity equilibrium at time equal to zero, convective flow vanishes. Therefore, from Darcy's law:

$$\rho_p \frac{kk_{rp}}{\mu_p}\left(\nabla p_p - \gamma_p \nabla D\right) = 0 \qquad p = \text{gas, oil, and water.} \tag{15}$$

For a horizontal plane $\nabla D = 0$, so equation (15) simplifies to:

$$\frac{\partial p_p}{\partial x} = 0, \tag{16}$$

$$\frac{\partial p_p}{\partial y} = 0. \tag{17}$$

Equations (16) and (17) show that pressure, composition, and saturation are constant in a horizontal plane at time equal to zero. For the vertical direction, equation (15) becomes:

$$\frac{\partial p_p}{\partial z} - \gamma_p = 0. \tag{18}$$

Equation (18) means that vertical pressure distribution is given by the column weight.

Integrating equation (18) results in:

$$p_p = p_{\text{ref}} + \bar{\gamma}_p (z - z_{\text{ref}}), \tag{19}$$

where $\bar{\gamma}_p$ is the average specific weight of phase p between z and z_{ref} heights. If pressure at a reference height is given, then pressure at any point in the model can be calculated from equation (19).

5.2 Matrix boundary conditions

There are two boundary condition types for the matrix: 1-matrix sealed boundary condition and 2-matrix-fracture boundary condition (Fig. 1). These boundary conditions are attended as follows:

5.2.1 Matrix sealed boundary conditions

The total mass flux for all components in all phases vanishes at these boundaries. That is:

Convection flux at the boundary:

$$\rho_p \frac{kk_{rp}}{\mu_p}\left(\nabla p_p - \gamma_p \nabla D\right) = 0. \tag{20}$$

Diffusion flux at the boundary:

$$\phi S_p \rho_p (D_{c,p} \nabla x_c) = 0 \qquad c = 1, 2, \ldots, nc. \tag{21}$$

5.2.2 Matrix-fracture boundary conditions

The continuity equation in the fracture includes mass transport by diffusion and convection mechanisms in a laminar flow regime. The diffusion mass transfer rate at matrix-fracture surface is found by:

$$q_{D,fm,c} = A\rho_g D_{e,c}\left(\frac{\partial y_c}{\partial z}\right)_{z=0} \qquad c = 1, 2, \ldots, n_c, \tag{22}$$

where ρ_g is gas stream density in the fracture.

Convection between a matrix grid cell and the adjacent fracture ($q_{C,fm,c}$) is defined in the model based on Darcy's law as:

See the equation (23) bottom of the page

6 Numerical Solution of equations

The numerical model of the resulting equation has been discretized using the IMplicit Pressure Explicit Saturation (IMPES) approach. We obtain the pressure implicitly and the saturation explicitly. Some of the equations in the multiphase compositional flow in the porous media are nonlinear. Therefore, using numerical methods, we substitute finite difference approximations in a nonlinear equation system for all derivatives. The equations are then linearized and solved using MATLAB software.

6.1 Validation of model

The mathematical model has been validated using laboratory data of Morel *et al.* [48], Le Romancer and Fernandes [49]. N_2 was injected in the first experiment and in the second experiment, CO_2 was injected into the porous media

The matrix residual oil is C_1 and C_5 mixture. In the N_2 injection experiment, the oil and vapour phases were present initially, but in the experiment of CO_2 injection, the matrix was saturated with the oil phase. Experiments were carried out in a one-dimensional system to simulate the mass transfer between a gas in a fracture (N_2 or CO_2) and a residual oil (C_1–C_5). The injected gas (N_2 or CO_2) diffuses into the residual oil in the porous matrix and

$$q_{C,fm,c} = \left(x_c \rho_o \frac{kk_{ro}}{\mu_0}\right)_{\text{matrix}} \left[\left(\nabla p_o - \gamma_o \nabla D\right)_{\text{matrix}} - \left(\nabla p_g - \gamma_g \nabla D\right)_{\text{fracture}}\right] + \left(y_c \rho_g \frac{kk_{rg}}{\mu_g}\right)_{\text{matrix}} \left[\left(\nabla p_g - \gamma_g \nabla D\right)_{\text{matrix}} - \left(\nabla p_g - \gamma_g \nabla D\right)_{\text{fracture}}\right]. \tag{23}$$

evaporates the oil by convection and diffusion. The diffusion process alters the composition of the core fluid, resulting in changes in the phase's properties such as density. Recovery of each component (C_1–C_5) during the matrix was obtained in both experiments.

6.2 Simulation of N_2 injection test

First, explanation of the N_2 injection experiment is presented followed by the results of mathematical model. Tables 1 and 2 show the model parameters and the relative permeability and capillary pressure, respectively. N_2 injection experiments were performed in a one-dimensional horizontal core by Morel *et al.* [48]. Figure 2 demonstrates the setup of the experiment.

All parts of the core were insulated except one side where N_2 gas enters from. The sample of the *Paris Basin Chalk* was used as the core. N_2 was injected at an initial pressure of 1479 Psi, initial temperature of 38.5 °C and the composition (C_1 (52.4 mole%) – C_5 (47.6 mole%)) were assumed constant. At the start of the experiment, the porous matrix containing a combination of C_1 and C_5 is distributed between the equilibrium liquid and gas phases. A gas with an initial saturation of 25% is presented within the matrix. Injected N_2 diffuses into the gas phase and solves at the boundary between the fracture and the matrix in the liquid phase. The pressure at the fracture-core boundary is fixed throughout the simulation and compositions are uniform along the core. The core is simulated with 20 grids in the x direction. The capillary pressure of gas–oil is corrected to a reference surface tension.

Nitrogen injection experiment was performed for 16 days and the simulation of the experiment was intended for 30 days. To better understand the importance of molecular diffusion in recovery, testing and simulation have been done in two ways:

A – Regardless of the convection at the boundary of matrix-fracture (or $q_{C,\ fm,c} = 0$).
B – Considering the convection at the boundary of matrix-fracture.

The magnitude of the mechanisms of diffusion and convection in transfer of each component into the core is depicted in Figures 3a–3d. The positive sign in these figures means the mass transfer from the boundary of fracture-core to the core and the negative sign means the transfer of mass from the matrix to the boundary of fracture-core. The mass transfer of N_2 from the fracture to the core causes a counter-current flow to the core. Figures 3a–3d reveal that N_2 is transferred to the end of the core by the gas convection and molecular diffusion from the boundary of fracture-core (positive values). The counter-current flow of the oil, from the end of the core to the fracture-core boundary, makes the N_2 to move to the fracture boundary by convection (negative values). Figures 3a and 3b depict that at the beginning of simulation, no matter whether the matrix-fracture boundary conditions are without convection (state A) or with convection (state B), N_2 is mainly transported in the gas phase into the core by molecular diffusion. Figure 3c describes if the convection between the matrix and the fracture is ignored (state A), then the molecular diffusion of the gas will stay as the dominant mechanism of N_2 transfer into the core for 28 days. But if the convection between the matrix and the fracture is considered (state B), then gas convection will be the dominant mechanism for mass transfer in 28 days (Fig. 3d).

Figures 4a–4d measure the value of convection and diffusion mechanisms of oil and gas in transfer of C_1 into the core. C_1 reaches to the boundary of fracture-core through the gas and oil phases and transported to the oil phase by convection (negative values). The gas flow that is moving

Table 1. Inputs of model for simulation of the experiment of N_2 injection.

Core properties	Paris Basin Chalk
Length of the core (m)	0.375
Cross section of the core (m^2)	0.064 × 0.064
Porosity of the core (%)	40
Permeability of the core (mD)	2
Saturation of the water (%)	0
Saturation of the residual oil (%)	0.2

Table 2. Relative permeability and capillary pressure [21].

P_{cog}, kPa	K_{rg}	K_{ro}	S_g
15.366	0	1	0
16.235	0.0002	0.9	0.1
17.105	0.004	0.586	0.2
17.975	0.02	0.316	0.3
18.700	0.045	0.153	0.4
19.569	0.1	0.063	0.5
20.222	0.15	0.037	0.55
20.874	0.21	0.02	0.6
21.744	0.3	0.0096	0.65
22.607	0.5	0.0039	0.7
27.542	0.9	0	0.8

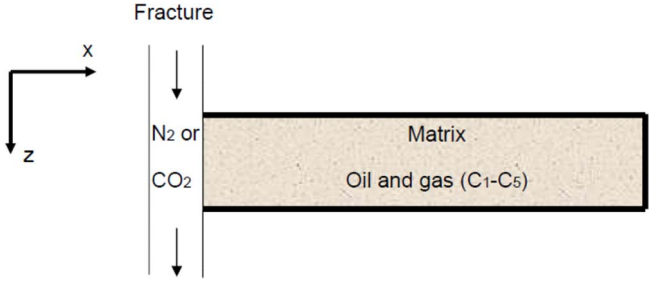

Fig. 2. Morel *et al.* experiment layout.

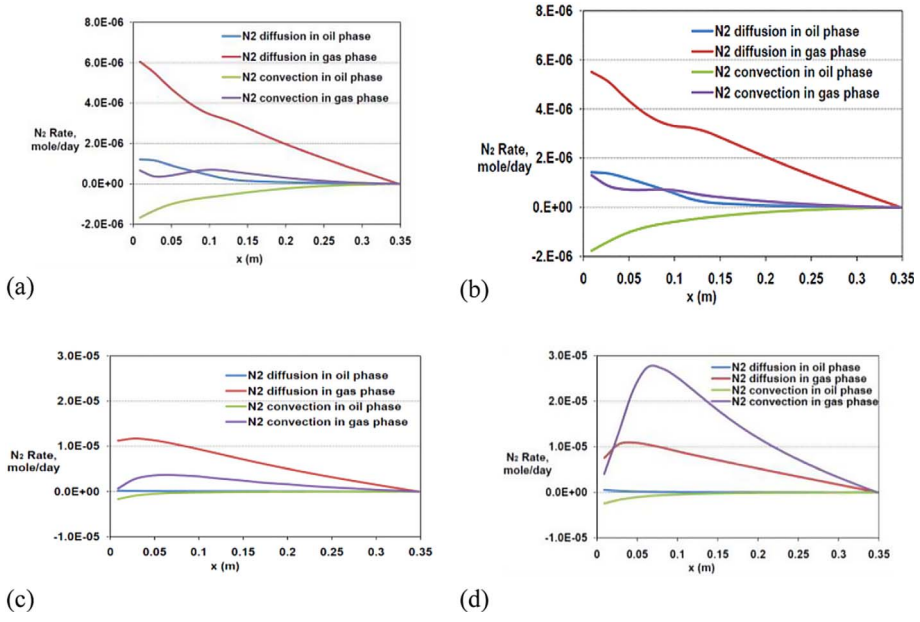

Fig. 3. Calculation of N_2 rate in matrix in N_2 injection experiment at: (a) $t = 8$ days state A, (b) $t = 8$ days state B, (c) $t = 28$ days state A, (d) $t = 28$ days state B.

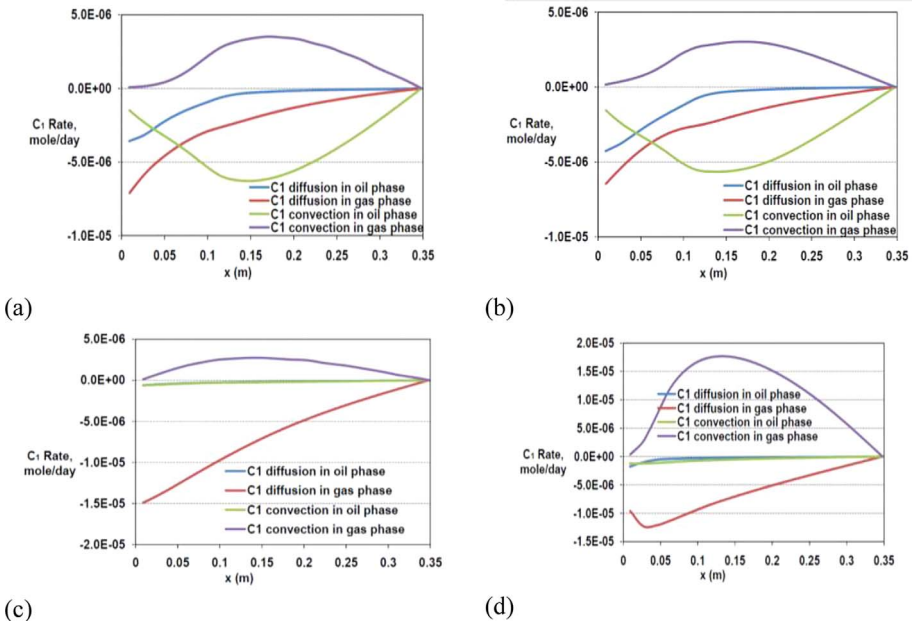

Fig. 4. Calculation of C_1 rate in matrix in N_2 injection experiment at: (a) $t = 8$ days state A, (b) $t = 8$ days state B, (c) $t = 28$ days state A, (d) $t = 28$ days state B.

from the boundary of fracture-core to the end of the core, moves methane in the reverse direction. Figures 4a and 4b show that for both matrix-fracture boundary conditions, without convection (state A) and with convection (state B), at the beginning of test times ($t = 8$ days), C_1 is mainly transmitted by molecular diffusion into the core because convection in the oil and gas phases moves C_1 in the reverse direction and finally neutralizes each other. If the movement between the matrix and the fracture is ignored (state A) the molecular diffusion of the gas stays the dominant mechanism of transport (Fig. 4c). However, Figure 4d reveals that at the end of times, gas convection is the most

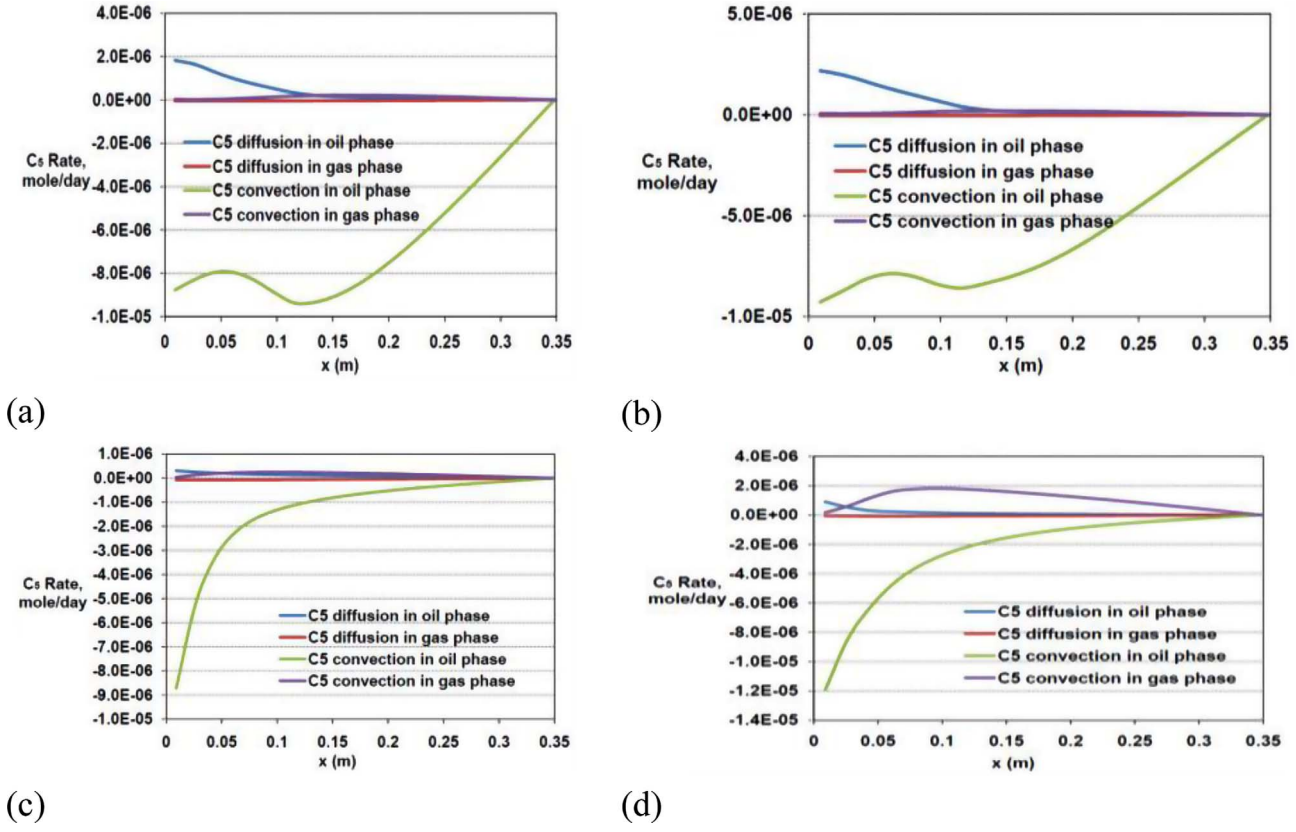

Fig. 5. Calculation of C_5 rate in matrix in N_2 injection experiments at: (a) $t = 8$ days state A, (b) $t = 8$ days state B, (c) $t = 28$ days state A, (d) $t = 28$ days state B.

important factor for transferring of C_1 from boundary to the core with considering convection between the matrix and the fracture in state B.

Figures 5a–5d confirm that oil convection, disregarding to convection (state A) or considering convection (state B) between the matrix and the fracture, is the predominant factor of C_5 movement from the end of the core to the boundary of fracture-core. It is also the significant mechanism of pentane transport into the core for the whole simulation time.

It is obvious that C_1 recovery is greater than C_5 (because C_1 is the lighter component and also more mobile than the C_5, which is a heavier component), as shown in Figure 6. Over time, the percentage of components recovery increases. For example, for component C_1 in state A, the recovery percentage has risen from 20% on the 5th day to about 43% on the 20th day. Recovery of both components C_1 and C_5 in state A (without convection) and in state B (with convection) shows that diffusion compared with convention has a crucial role in recovery of oil components. At the beginning of the simulation, the diffusion mechanism is the main recovery mechanism, but over time, the role of the convection mechanism in C1 recovery increases and this is the reason that why after $t = 25$ days, the boundary conditions of A and B no longer match together. Figures 7a–7c show saturated changes in 4, 8, and 16 days after starting the process. The differences between the modeling and

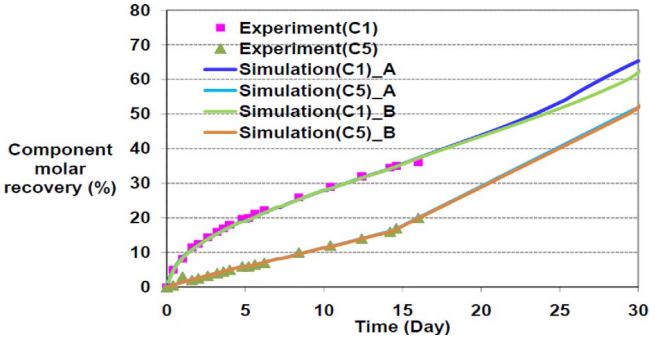

Fig. 6. Calculated and experimental C_1 and C_5 recoveries in N_2 injection experiment.

experimental results are acceptable. At the beginning of the injection operation, at $t = 4$ days, the saturation of the gas inside the core is high and nitrogen has not yet been able to completely replace the gas inside the core. As the injection time increases, more nitrogen diffuses into the pores of the core and replaces the gas inside the core, reducing the percentage of gas saturation. At $t = 4$ days, the maximum saturation percentage for state A is 65%, while at $t = 8$ days, this value reaches to 55%. Also, at the end of the core, the percentage of gas saturation is high and less nitrogen has diffused to the end of the core. At $t = 16$ days,

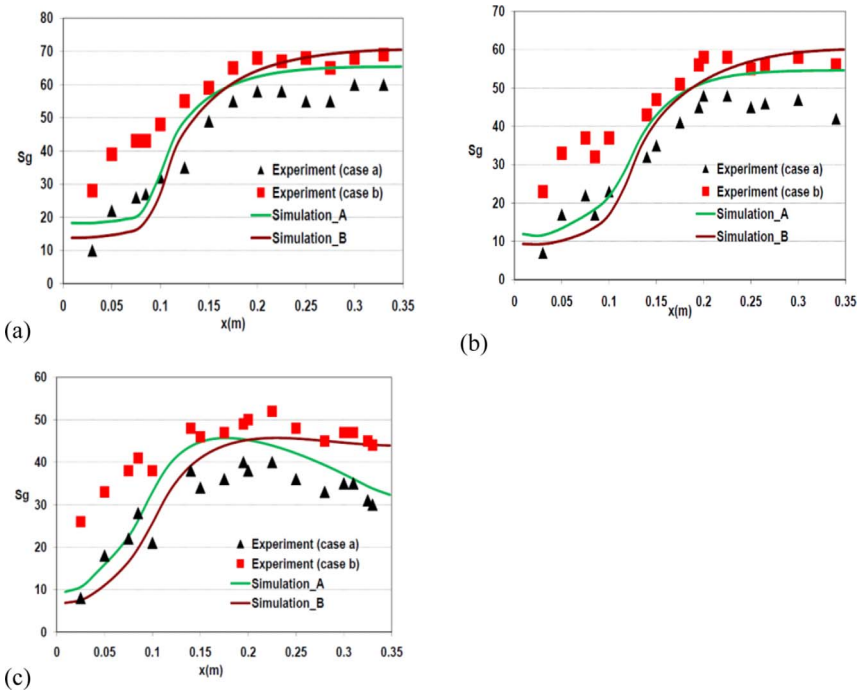

Fig. 7. Gas saturation in N_2 injection experiment at: (a) $t = 4$ days, (b) $t = 8$ days, (c) $t = 16$ days.

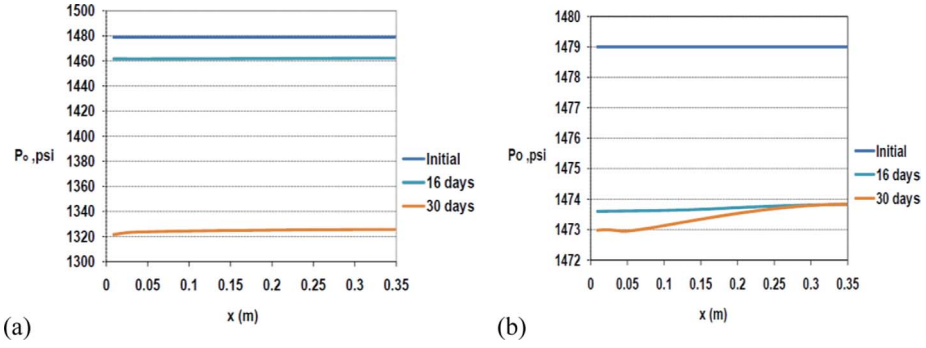

Fig. 8. Oil pressure distribution in N_2 injection experiment. (a) State A, (b) state B.

Table 3. Model inputs for CO_2 injection.

Saturation of the water (%)	11
Pressure (kPa)	6300
Temperature (K)	311.65
Initial saturation of gas (%)	0
Mole fraction of C_5	0.72
Flow rate of CO_2 in the fracture (cm^3/s)	4

the rate of gas saturation is 45% which is lower than in previous times. As we move to the end of the core, the percentage of gas saturation is higher as nitrogen has not been able to move to the end of the core. As nitrogen travels through the core due to pores inside the core, gases move to the end of the core and accumulate there as a result the percentage of gas saturation at the end of the core increases. The main

Table 4. The specifications of the core.

Core thickness (m)	3.19E–02
Core width (m)	3.19E–02
Core length (m)	0.357E–01
Porosity (%)	4.000E–01
Pore volume (m^3)	1.46E–04
C_1 initial mole fraction	0.28
C_5 initial mole fraction	0.72
MW oil	56.44
Oil density (kg/m^3)	566.87
Oil density (mol/m^3)	10.04
Oil saturation (S_o)	0.89
Oil initial total mole	1.30E–03
C_1 initial total mole	3.65E–04
C_5 initial total mole	9.37E–04

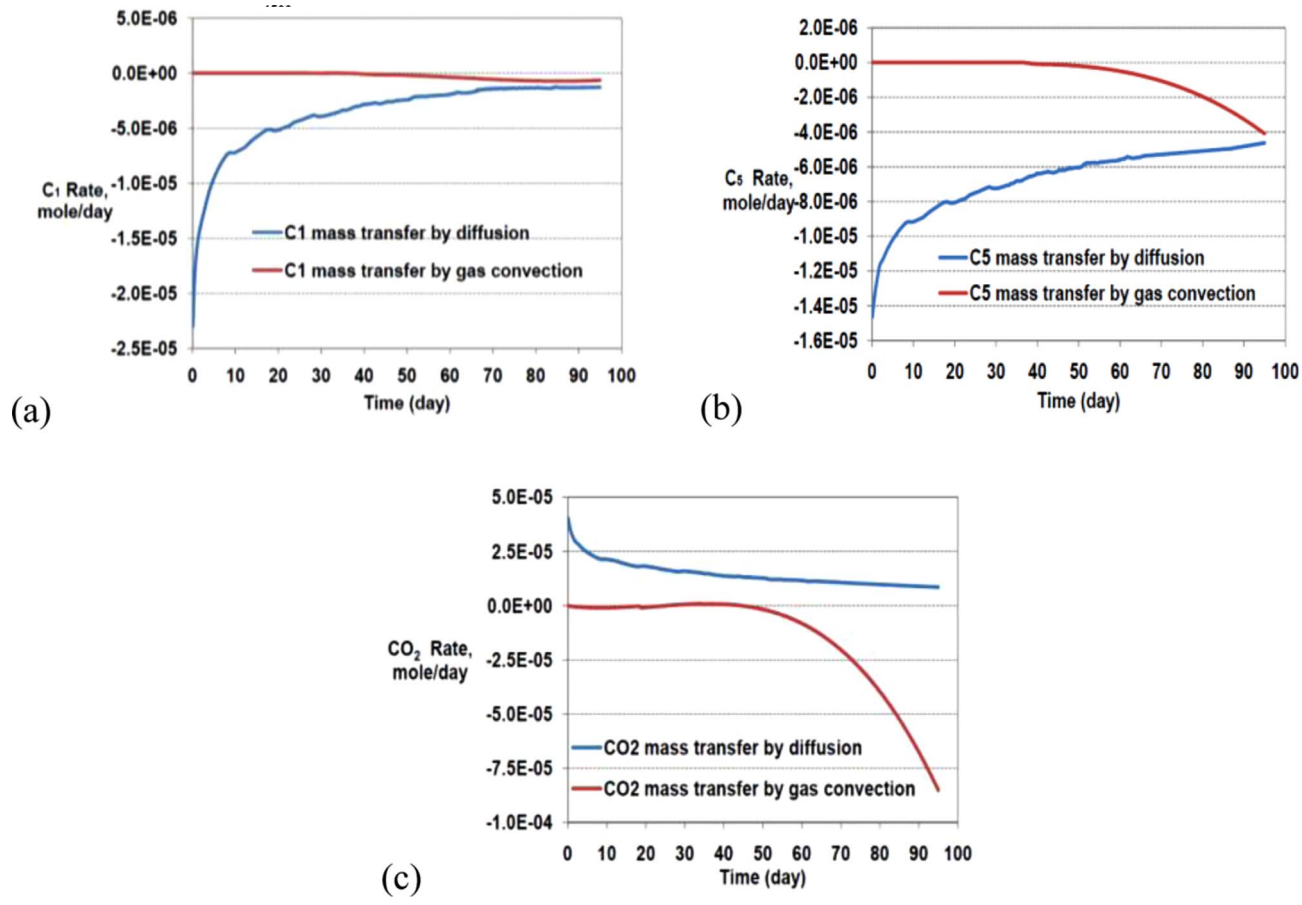

Fig. 9. Calculation of mass transfer rate at fracture-matrix surface in CO_2 injection experiment. (a) CO_2 mass transfer rate, (b) C_1 mass transfer rate, (c) C_5 mass transfer rate.

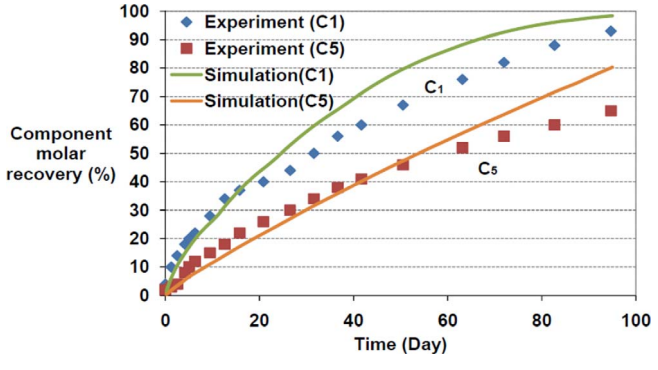

Fig. 10. Calculated and experimental C_1 and C_5 recoveries in CO_2 injection experiment.

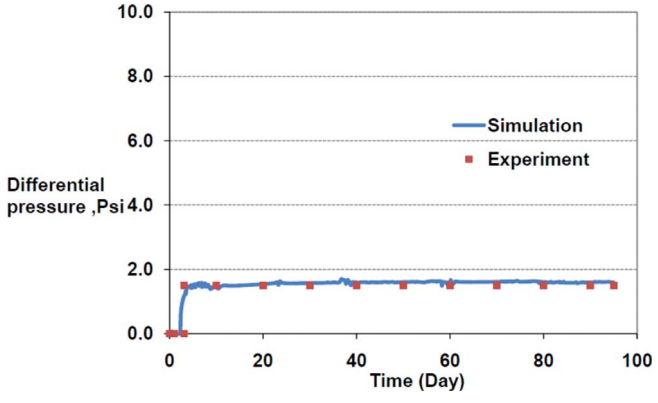

Fig. 11. Differential pressure between matrix and fracture in CO_2 injection experiment.

reason for the reduction in reservoir pressure is the release of oil-soluble gas. The pressure created by the gravity drainage mechanism keeps soluble the gas in the oil and maintains the pressure of reservoir. Figures 8a and 8b show the pressure of oil changes at the matrix-fracture boundary in the core for two states without and with convection, (A) and (B) respectively. Figure 8a demonstrates a significant drop in oil pressure from 1479 Psi at $t = 0$ day to 1320 Psi at $t = 30$ days when convection is ignored at boundary between matrix and fracture, While Figure 8b demonstrates that the convection of N_2 from the fracture into the matrix results the pressure of the core to stay constant around 1473 Psi for $t = 30$ days. Therefore, the presence of a convection mechanism prevents oil pressure to drop. Comparing Figures 8a and 8b, in the presence

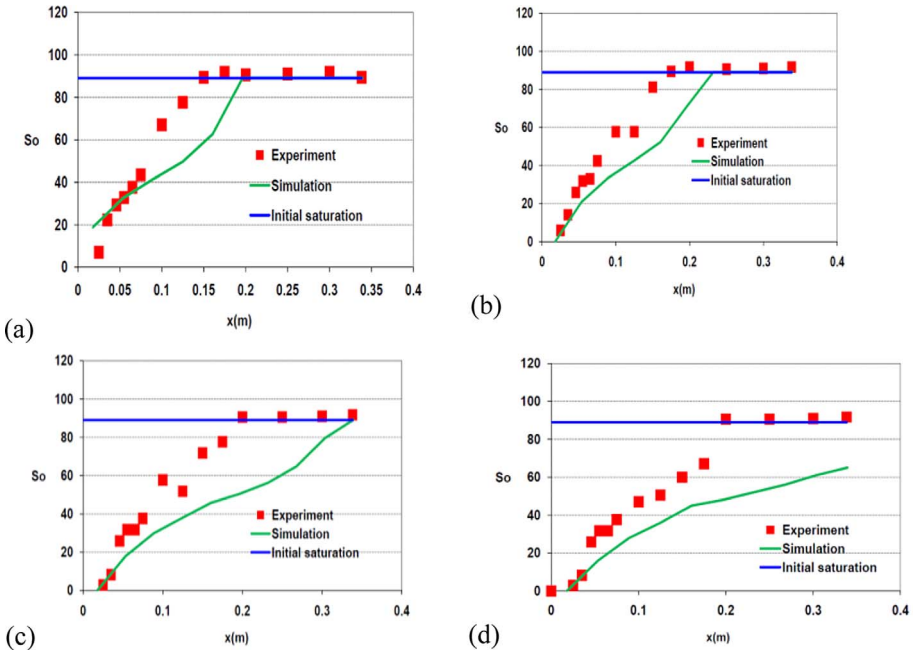

Fig. 12. Oil saturation in CO_2 injection experiment at: a) $t = 53$ days, (b) $t = 67$ days, (c) $t = 88$ days, (d) $t = 95$ days.

of convection (state B), the pressure drop at $t = 30$ days has finally reached from 1479 Psi to 1473 Psi, but without convection (state A) the pressure drop after $t = 30$ days, from 1479 Psi to 1320 Psi, it shows the great importance of the convection mechanism in preventing reservoir pressure drop.

6.3 Simulation of CO_2 injection experiments

Next, the mathematical model is investigated for CO_2 injection into the fractured reservoir and results are compared with experimental data carried out by Le Romancer and Fernandes [49]. In this case also, all the core surfaces except one is insulated. The *Paris Basin Chalk* was used as the matrix. CO_2 was injected into the fracture at a temperature of 38.5 °C and pressure of 913.74 Psi. The matrix was saturated with a liquid phase of 28 mole% of C_1 and 72 mole% of C_5 in this test. Initially, the core has no gas saturation and there is an aqueous phase residing at 11% saturation in the core and the initial saturation of the gas is 0%, which is assumed to be constant throughout the core. The core is simulated in the x direction by 10 grids and at the fracture-core boundary. Model inputs for simulating of CO_2 injection experiments are given in Table 3. The specifications of the core in this experiment are presented in Table 4.

Figures 9a–9c show the mass transfer of CO_2, C_1, and C_5 at the matrix-fracture boundary by the convection and gas diffusion mechanisms. Figure 9a proves that approximately 40 days after the start of the experiment, the CO_2 is transferred to the matrix-fracture boundary predominantly by diffusion. After 40 days, CO_2 leaves the core by the convection of gas phase and entering the fracture-core boundary by diffusion mechanism. The difference between the rate of gas convection and the CO_2 diffusion at the boundary of fracture-core increases with time. Figure 9b indicates that C_1 at the boundary of fracture-core is recovered mostly by diffusion about 40 days after the beginning of the experiment, while the gas convection begins to transfer C_1 from the boundary of fracture-core to the fracture after 40 days. In C_1 recovery after 70 days, mass transfer by gas convection and diffusion at the fracture-core boundary has the same importance. Figure 9c depicts that diffusion at the surface of fracture-core is the most substantial mechanism for C_5 recovery for up to 40 days. While the convection of gas from fracture-core to the fracture starts to participate in C_5 recovery after 40 days. Although recovery of C_5 with gas convection increases over time, C_5 transport by diffusion will remain as a significant mechanism. Like N_2 injection experiment, C_1 recovery is higher than the C_5 recovery (Fig. 10) and over time, the percentage of components recovery increases. Figure 11 proves the difference pressure between the fracture-matrix boundary. Due to the difference in the permeability of the fracture and the core, the pressure difference increases sharply and then remains at a constant value. The agreement between the experimental data and the obtained results from the model is acceptable. The pressure in the core drops sharply in the lack of convection between the fracture and the matrix. Figures 12a–12d compare saturated changes in 53, 67, 88, and 95 days. The more time passes from the start of injection, the oil saturates in the farther distance from the beginning of the core. For example, at $t = 53$ days, the oil reaches maximum saturation in $x = 0.22$ m from the beginning of the core. At $t = 88$ days, this distance is equal to $x = 0.34$ m. Also, this distance increases with the duration of the injection operation. Because saturation of water in

the core is constant (11%), saturation of oil will not be higher than 89%. Figures 12a–12d show that the gas in the simulation results are more than experimental data.

7 Conclusion

Diffusion is the most important mechanism of mass transfer during N_2 injection between the matrix and the fracture. In the early simulation times, N_2 and C_1 are predominantly transported into the core by molecular diffusion of gas while C_5 is transferred into the core principally by oil convection. Moreover, during CO_2 injection test, diffusion and convection are both considerable. At the onset of the simulation, the diffusion mechanism is the dominant recovery mechanism, but over time, the role of the convection mechanism in C_1 and C_5 recovery increases. In addition, light component recovery is more than heavy component recovery. After 28 days of N_2 injection test, the lighter component recovery is about 50%, and the heavier component is recovered about 40%. Over time, the percentage of components recovery increases.

During N_2 injection experiment, at the primary simulation times, N_2 and C_1 are mainly transported into the core by molecular gas diffusion, and the role of the convection mechanism increases as the simulation is proceeded. C_5 is transferred into the core mostly by oil convection. Thus, for each component the mechanism of transport depends on the boundary conditions of matrix-fracture (state A or state B). For state A, boundary conditions of the fracture-matrix, gas molecular diffusion remains the most important mechanism in the transfer of N_2 and C_1 into the core at the simulation end times. Moreover, for state B, gas convection is the most important mechanism for the transfer of N_2 and C_1 into the core at the end of the simulation. Also, oil transfer, regardless of the boundary conditions between the matrix and the fracture (state A or state B), is the most important mechanism of C_5 transport into the core for the entire simulation time.

Ultimately, it is found that during the initial simulation times, when CO_2 is injected, CO_2, C_1, and C_5 are often transported into the core by the diffusion of oil and gas. In addition, the convection of oil and gas in the transfer of CO_2, C_1, and C_5 into the core increases with time, but the role of the diffusion mechanism during the simulation cannot be ignored.

As the time of nitrogen injection into the core increases, the maximum percentage of gas saturation in the core decreases and more gas escapes from the pores of the core. The convection mechanism has a great effect on preventing the pressure drop of the reservoir during injection operations.

Supplementary materials

The supplementary of this article is available at https://ogst.ifpenergiesnouvelles.fr/10.2516/ogst/2021065/olm

Solution method (Supplementary material).doc
Matlab code (Supplementary material).rar
Flow chart (Supplementary material)

References

1 Mai A., Kantzas A. (2009) Heavy oil waterflooding: effects of flow rate and oil viscosity, *J Can Pet Technol* **48**, 42–51.
2 Santos R.G., Loh W., Bannwart A.C., Trevisan O.V. (2014) An overview of heavy oil properties and its recovery and transportation methods, *Brazilian J. Chem. Eng.* **31**, 571–590.
3 Babadagli T. (2003) Evaluation of EOR methods for heavy-oil recovery in naturally fractured reservoirs, *J. Pet. Sci. Eng.* **37**, 25–37.
4 Hoteit H., Firoozabadi A. (2006) *Numerical modeling of diffusion in fractured media for gas injection and recycling schemes*, Society of Petroleum Engineers.
5 Fan J., Qu X., Wang C., Lei Q., Cheng L., Yang Z. (2016) Natural fracture distribution and a new method predicting effective fractures in tight oil reservoirs in Ordos Basin, NW China, *Pet. Explor. Dev.* **43**, 806–814.
6 Yun Z., Jianfang S., Zhongchun L. (2019) Study of numerical simulation method modelling gas injection into fractured reservoirs, *Min. Miner. Depos.* **13**, 41–45.
7 Bratton T., Canh D.V., Van Que N., Duc N.V., Gillespie P., Hunt D., Li B., Marcinew R., Ray S., Montaron B., Nelson R., Schoderbek D., Sonneland L. (2006) The nature of naturally fractured reservoirs, *Oilf. Rev.* **18**, 4–23.
8 Saidi A.M. (1983) Simulation of naturally fractured reservoirs, in: *SPE Reservoir Simulation Symposium*, Society of Petroleum Engineers.
9 Narr W. (2011) *Characterization of naturally fractured reservoirs*, Society of Petroleum Engineers.
10 Sarma P., Aziz K. (2006) New transfer functions for simulation of naturally fractured reservoirs with dual porosity models, *SPE J* **11**, 328–340.
11 Jamialahmadi M., Emadi M., Müller-Steinhagen H. (2006) Diffusion coefficients of methane in liquid hydrocarbons at high pressure and temperature, *J. Pet. Sci. Eng.* **53**, 47–60.
12 Zhang X., Jeffrey R.G., Thiercelin M. (2009) Mechanics of fluid-driven fracture growth in naturally fractured reservoirs with simple network geometries, *J. Geophys. Res. Solid Earth* **114**, B12.
13 Bagheri M.A., Settari A. (2008) Modeling of geomechanics in naturally fractured reservoirs, *SPE Reserv. Eval. Eng.* **11**, 108–118.
14 Lemonnier P., Bourbiaux B. (2010) Simulation of naturally fractured reservoirs. State of the art: Part 1 – physical mechanisms and simulator formulation, *Oil Gas Sci. Technol. – Rev. IFP Energies nouvelles* **65**, 239–262.
15 Lemonnier P., Bourbiaux B. (2010) Simulation of naturally fractured reservoirs. State of the art: Part 2 – Matrix-fracture transfers and typical features of numerical studies, *Oil Gas Sci. Technol. – Rev. IFP Energies nouvelles* **65**, 263–286.
16 Zheng S. (2016) Enhanced heat and mass transfer for alkane solvent (s)-CO_2-heavy oil systems at high pressures and elevated temperatures, *Ph.D. Thesis*, Petroleum Systems Engineering, University of Regina.
17 Trivedi J.J., Babadagli T. (2009) Oil recovery and sequestration potential of naturally fractured reservoirs during CO_2 injection, *Energy Fuels* **23**, 4025–4036.
18 Al-Kobaisi M., Kazemi H., Ramirez B., Ozkan B., Atan S. (2007) A critical review for proper use of water-oil-gas transfer functions in dual-porosity naturally fractured reservoirs – Part II, in: *International Petroleum Technology Conference*, European Association of Geoscientists & Engineers.

19 Song Z., Song Y., Li Y., Bai B., Song K., Hou J. (2020) A critical review of CO_2 enhanced oil recovery in tight oil reservoirs of North America and China, in: *SPE/IATMI Asia Pacific Oil & Gas Conference And Exhibition*, OnePetro.

20 Fang X., Yue X., Fang W., Lu S., Geng Z. (2017) EOR simulation of convection and diffusion in fracture during CO_2 injection in tight oil reservoir, in: *SPE Reservoir Characterisation and Simulation Conference and Exhibition*, Society of Petroleum Engineers.

21 Hu H., Whitson C.H., Qi Y. (1991) A study of recovery mechanisms in a nitrogen diffusion experiment, in: *IOR 1991-6th European Symposium on Improved Oil Recovery*, European Association of Geoscientists & Engineers, pcp-44.

22 Shojaei H. (2014) Mass transfer during enhanced hydrocarbon recovery by gas injection processes, *PhD Thesis*, University of Southern California.

23 Riazi M.R., Whitson C.H., Da Silva F. (1994) Modelling of diffusional mass transfer in naturally fractured reservoirs, *J. Pet. Sci. Eng.* **10**, 239–253.

24 Chordia M., Trivedi J.J. (2010) Diffusion in naturally fractured reservoirs: a review, in: *SPE Asia Pacific Oil and Gas Conference and Exhibition*, Society of Petroleum Engineers.

25 Saki M., Masihi M., Shadizadeh S.R. (2015) An improved mathematical model for mass transfer in fractured reservoir-during gas injection process, *Sci. Iran.* **22**, 955–966.

26 Ertekin T., King G.A., Schwerer F.C. (1986) Dynamic gas slippage: a unique dual-mechanism approach to the flow of gas in tight formations, *SPE Form. Eval.* **1**, 43–52.

27 Ayala L.F., Ertekin T., Adewumi M. (2005) Compositional Modeling of Retrograde Gas-Condensate Reservoirs in Multimechanistic Flow Domains, in: *Presented at the SPE Latin American and Caribbean Petroleum Engineering Conference, Rio de Janeiro, Brazil, June 2005.*

28 Karimaie H. (2007) Aspects of water and gas injection in fractured reservoirs.

29 Kazemi A., Jamialahmadi M. (2009) The effect of oil and gas molecular diffusion in production of fractured reservoir during gravity drainage mechanism by CO_2 injection, in: *EUROPEC/EAGE Conference and Exhibition*, Society of Petroleum Engineers.

30 Alavian S.A. (2011) Modeling CO_2 injection in fractured reservoirs using single matrix block systems, *PhD Thesis*, Norwegian University of Science and Technology, Trondheim, October 2011.

31 Hoteit H. (2013) Modeling diffusion and gas–oil mass transfer in fractured reservoirs, *J. Pet. Sci. Eng.* **105**, 1–17.

32 Mohebbinia S., Wong T. (2017) Molecular diffusion calculations in simulation of gasfloods in fractured reservoirs, in: *SPE Reservoir Simulation Conference*, Society of Petroleum Engineers.

33 Darvish H., Hemmati N., Naghshgar A., Tabzar A. (2019) Study of CO_2 molecular diffusion effect on the production of fractured reservoirs: The role of matrix porosity, and a new model for predicting the oil swelling factor, *Eur. Phys. J. Plus.* **134**, 1–14.

34 Jin L., Hawthorne S., Sorensen J., Pekot L., Kurz B., Smith S., Heebink L., Herdegen V., Bosshart N., Torres J., Dalkhaa C., Peterson K., Gorecki C., Steadman E., Harju J. (2017) Advancing CO_2 enhanced oil recovery and storage in unconventional oil play – experimental studies on Bakken shales, *Appl. Energy* **208**, 171–183.

35 Alipour Tabrizy V. (2014) Investigation of enhanced oil recovery using dimensionless groups in wettability modified chalk and sandstone rocks, *J. Pet. Eng.* **2014**, 430309.

36 Grogan A.T., Pinczewski W.V. (1987) The role of molecular diffusion processes in tertiary CO_2 flooding, *J. Pet. Technol.* **39**, 591–602.

37 Yang C., Gu Y. (2005) A novel experimental technique for studying solvent mass transfer and oil swelling effect in the vapour extraction (VAPEX) process, in: *Canadian International Petroleum Conference*, Petroleum Society of Canada.

38 Butler R.M., Mokrys I.J. (1991) A new process (VAPEX) for recovering heavy oils using hot water and hydrocarbon vapour, *J. Can. Pet. Technol.* **30**. https://doi.org/10.2118/91-01-09

39 Li X., Yortsos Y.C. (1995) Theory of multiple bubble growth in porous media by solute diffusion, *Chem. Eng. Sci.* **50**, 1247–1271.

40 Da Silva F.V., Belery P. (1989) Molecular diffusion in naturally fractured reservoirs: a decisive recovery mechanism, in: *SPE Annual Technical Conference and Exhibition*, Society of Petroleum Engineers.

41 Ghorayeb K., Firoozabadi A. (2000) Numerical study of natural convection and diffusion in fractured porous media, *SPE J.* **5**, 12–20.

42 Darvish G.R., Lindeberg E.G.B., Holt T., Kleppe J., Utne S. A. (2006) Reservoir conditions laboratory experiments of CO_2 injection into fractured cores, in: *SPE Europec/EAGE Annual Conference and Exhibition*, Society of Petroleum Engineers.

43 Yanze Y., Clemens T. (2012) The role of diffusion for nonequilibrium gas injection into a fractured reservoir, *SPE Reserv. Eval. Eng.* **15**, 60–71.

44 Moortgat J., Firoozabadi A. (2013) Fickian diffusion in discrete-fractured media from chemical potential gradients and comparison to experiment, *Energy Fuels* **27**, 5793–5805.

45 Wan T., Sheng J.J., Watson M. (2014) Compositional modeling of the diffusion effect on EOR process in fractured shale oil reservoirs by gas flooding, in: *Unconventional Resources Technology Conference, Denver, Colorado, 25-27 August 2014*, Society of Exploration Geophysicists, American Association of Petroleum, pp. 2248–2264.

46 Zuloaga-Molero P., Yu W., Xu Y., Sepehrnoori K., Li B. (2016) Simulation study of CO_2-EOR in tight oil reservoirs with complex fracture geometries, *Sci. Rep.* **6**, 1–11.

47 Bird R.B., Stewart W.E., Lightfoot E.N. (2006) *Transport phenomena*, John Wiley & Sons.

48 Morel D.D., Bourbiaux B., Latil M., Thiebot B. (1990) Diffusion effects in gas-flooded light oil fractured reservoirs. SPE 20516, in: *SPE Annual Technical Conference and Exhibition, New Orleans, LA, September*, pp. 23–26.

49 Le Romancer J.F., Fernandes G. (1994) Mechanism of oil recovery by gas diffusion in fractured reservoir in presence of water, in: *SPE/DOE Improved Oil Recovery Symposium*, Society of Petroleum Engineers.